Effective Non-Iterative Phase Retrieval of 2-D Bandlimited Signals with Applications to Antenna Characterization and Diagnostics

Effective Non-Iterative Phase Retrieval of 2-D Bandlimited Signals with Applications to Antenna Characterization and Diagnostics

Giada M. Battaglia, *Member, IEEE,* Andrea F. Morabito, Roberta Palmeri, *Member, IEEE*, and Tommaso Isernia, *Fellow, IEEE*

***Abstract*—The phase retrieval problem is dealt with for the challenging case where just a single set of (phaseless) field data is available. In particular, the adoption of a new set of intersecting curves in the spectral plane allows decisive improvements over our recent approaches emulating the solution of crosswords puzzles, thus removing relevant limitations on the source size. Numerical examples support the given theory and confirm the effectiveness of the developed procedure.**

***Index Terms*—Antenna characterization, antenna diagnostics, phase retrieval, signal recovery.**

I. Introduction

As discussed in the related papers [1],[2], as well as in an extensive literature (see for example [3]-[24]), the so-called 'Phase Retrieval' (PR) problem is of interest in very many different branches of applied sciences, including antennas synthesis, diagnostics, and characterization. In such a kind of problems, one wants to retrieve a complex function from measurements of its square amplitude distributions plus some additional *a-priori* information.

In antenna applications, the function to be retrieved usually is (a component of) the radiated field, and the *a-priori* information is the support (and hence the location and dimensions) of the source generating such a field. Because of the Fourier-based relationship amongst the source and the far-field for both cases of discrete (i.e., array) and continuous aperture sources, particular attention has been devoted to the case where measurements are taken in the Fraunhofer zone. Consequently, the signal of interest can be considered bandlimited, with a bandwidth related to the size of the source [25].

This work was supported by the Italian Ministry of University and Research in part under the project 2017HZJXSZ entitled "CYBERPHYSICAL ELECTROMAGNETIC VISION: Context-Aware Electromagnetic Sensing and Smart Reaction" and in part under the project ARS01_01181 entitled "PM3- Piattaforma Modulare Multi-Missione".

T. Isernia, A. F. Morabito, and G. M. Battaglia are with DIIES Department, Università Mediterranea of Reggio Calabria, 89122 Reggio Calabria, Italy. R. Palmeri is with Institute for the Electromagnetic Sensing of the Environment of the National Council of Research (IREA-CNR), Via Diocleziano 328, 80124 Napoli, Italy. All authors are also with the National InterUniversity Consortium for Telecommunications (CNIT), Viale G.P. Usberti, 43124 Parma, Italy. T. Isernia is also with IREA-CNR, via Diocleziano 328, 80124 Napoli, Italy.

Corresponding author: Tommaso Isernia (tommaso.isernia@unirc.it)

Although PR has been the subject of very many papers, there is still the need of developing effective procedures for the canonical challenging case where the signal of interest is the Fourier transform of a 2-D signal having a finite support. In fact, existing (and generally iterative) solution procedures may get trapped into the so called 'false solutions' [26].

In our recent contributions [1],[2],[27] we tried to introduce new points of view. In particular, in [1],[2] we discussed two new procedures exploiting the solutions of 1-D PR problems and emulating the process of solving crossword puzzles.

Actually, as noticed from an unknown Reviewer, other approaches exploiting the solution of 1-D PR problem as a brick for 2-D PR had been already proposed in the literature [3],[4].

In particular, in [3] the authors proposed to solve a 1-D PR along a diameter of the spectral plane and then 'track' the complex zeroes of the polynomials associated to the different solutions by considering subsequent diameters corresponding to some small angular increments. While being intuitive, the method suffers from a number of relevant drawbacks. In fact, it is not able to take into account the multiplicity of solutions whenever one has to deal with factorable patterns. Moreover, the zeroes tracking may result a very difficult operation (especially when one or more zeroes cross the unitary circle in the complex plane).

In [4] 1-D PR problems are solved along columns and rows of the spectral plane, and then enforcement of consistency amongst the different 1-D distributions allows the desired 2-D reconstructions. Hence, in [1], which focuses on the case of array antennas, the basic idea is the same as the one in [4], but with two relevant differences in actual realization. First, in [1] we discuss and show the ability to deal with noisy data[1]. Second, we use the Spectral Factorization (SF) technique [28] of square amplitude distributions, rather than iteratively looking directly for the zeroes (which is a non-linear problem) as in [4].

This notwithstanding, [1] is affected by essentially the same limitations inherent to [4], i.e., the difficulties (inability) one encounters when dealing with large-order polynomials. As a matter of fact, such a difficulty is reported in all the very many

[1] Although in [4] the authors claim expected robustness with respect to noise, the (single-presented) example just deals with the noiseless case, and we were not able to find further contributions dealing with the noisy case.

papers (roughly 150) we found citing [3] or [4].

The problem has been partially overcome in [2] (which deals with continuous planar sources) where 1-D PR problems are supposed to be solved along diameters and concentric rings of the spectral plane. Then, initialization of the procedure using the smallest rings (where 1-D PR problems have just a few ambiguities) as well as some overlooked properties of the fields (and hybridization with [28]) allow the consideration of much larger sources, including the case where phaseless measurements are affected from noise. On the other side, one still needs to consider 1-D PR problems along diameters of the spectral plane and hence, in case of larger and larger sources, the corresponding 1-D PR have a huge number of possible solutions, with the inherent difficulties in discriminating amongst all of them.

In this contribution, we eliminate such a drawback by considering a third possibility dealing with (intersecting) curves of the spectral plane all having a small length and, by virtue of the band-limitedness property, corresponding to fields having a small amount of variability. As a consequence, the corresponding 1-D PR problems have a considerably reduced number of possible solutions, thus making much easier the crosswords processing and consequently the overall procedure.

Note that the chance we are pursuing, i.e., getting the actual 2-D complex field by a single set of phaseless data, is based on the theoretical uniqueness results arising from the fact that 2-D polynomials (but for a zero-measure set) are not factorable. This is indeed deeply different from the corresponding 1-D problem. In fact, in such a case the field and the square-amplitude distributions can be expressed as 1-D trigonometric polynomials, and the SF of the data can lead, through a 'zero flipping' procedure, to a large number of different complex fields all corresponding to the same power pattern (see [1],[2],[28] for more details).

Notably, in both the 1-D and 2-D cases, attention still must be paid to the so-called 'trivial ambiguities' affecting any PR problem (see [13] as well as Sect. IV of [2] for more details).

The paper is organized as follows. In Sect. II we recall field properties and representations useful for PR. Then, in Sect. III the basic idea enabling the proposed PR approach and the solution procedure are introduced. Finally, in Sect. IV the presented technique is assessed through different numerical experiments dealing with sources much larger than the ones affordable by our previous techniques. Conclusions follow.

II. Field Representation along (non-concentric) Rings

In Sect. III.B of [2] we gave an analysis of the properties and possible representations of the fields along (concentric) rings in the spectral domain. In particular, on the basis of the properties discussed in [29], we showed that, when considering electrically-large sources, an accurate representation for the spectrum along any circle of radius $\overline{k}$ centered in the origin of the spectral plane is given by:

$$F(\overline{k},\phi) = \sum_{\ell=-H}^{H} C_\ell(\overline{k}) e^{j\ell\phi} \tag{1}$$

where ϕ is the azimuth coordinate spanning the spectral domain and $H = \overline{k}a$ (a being the radius of the circular support of the source). More precisely, one has to consider $H = \lceil \overline{k}a \rceil$, where $\lceil x \rceil$ denotes the minimum integer larger than or equal to x.

A simple understanding of such a property can be given by noticing that a number of harmonics (and hence of samples) equal to $2\beta a + 1$ (β being the wavenumber) is required on the external circle of the visible range [29], and that the given solution for a generic circle is such to achieve the same sampling steps along the different circles.

As a suitable alternative, one can compute the Singular Value Decomposition (SVD) of the operator relating the aperture field to the ring at hand[2], which confirms that harmonics beyond $\lceil \overline{k}a \rceil$ are indeed negligible.

Notably, an expansion analogous to (1) holds true for the square amplitude distribution, the trivial difference being a doubling of the summation indices. In fact, following [28], the square-amplitude distribution data, say $M^2(\overline{k},\phi)$, can be conveniently represented as:

$$M^2(\overline{k},\phi) = \sum_{\ell=-2H}^{2H} D_\ell(\overline{k}) e^{j\ell\phi} \tag{2}$$

where D_ℓ is a Hermitian sequence.

Then, a key point of the procedure was expressing both (1) and (2) as the restriction to the unitary circle of a polynomial in the z-variable, i.e.:

$$F(\overline{k},\phi) = \sum_{\ell=-H}^{H} C_\ell(\overline{k}) z^\ell \tag{3}$$

$$M^2(\overline{k},\phi) = \sum_{\ell=-2H}^{2H} D_\ell(\overline{k}) z^\ell \tag{4}$$

so that, when $z = e^{j\phi}$, one turns back to (1) and (2).

In fact, such a circumstance and the fundamental theorem of algebra [31] allow the factorization of (4) and hence, by using the properties of the zeroes, the extraction of all the different possible expressions (1) and (3) for the field.

Notably, the order of the trigonometric polynomials (3) and (4) is smaller and smaller for decreasing values of $\overline{k}$, which allowed in [2] a solution procedure much more efficient than in [1].

Now, the very simple circumstance we rely upon herein is that bandlimitedness is a global property of the spectrum. Hence, representations (1)-(4) still hold true along rings which are not centered in the origin provided that the coefficients depend on the circle at hand and $\overline{k}$ is the radius of such a ring[3].

[2] Notably, by following the methodology in [30], this SVD can be computed in an analytical fashion.

[3] A simple way to prove that (3) and (4) hold true whatever the circle at hand is the fact that the fields (spectra) on a generic ring could be thought as

Such a circumstance provides definite advantages, eliminating the corresponding computational burden drawbacks of [2] in all steps of the crosswords-like processing way of thinking we had introduced.

III. The Basic Idea, and Development of the New Approach

This Section is devoted to present the devised approach. To this end, in the four following subsections we respectively describe the basic idea enabling the proposed method, the triggering and execution of the PR, the implementation details of the solution procedure, and the limitations inherent to the developed technique.

III.A. The basic idea and the adopted system of circles

Given the property recalled at the end of Sect. II, the basic idea is to exploit a system of concatenating rings. These latter should be such to:

a) cover the visible part of the spectrum;

b) have a number of intersection points allowing for an effective discrimination of solutions;

c) have a small radius, i.e., allowing to deal with low-order polynomials.

Obviously, very many different choices are possible. In the following, as we deem it very convenient, we take inspiration from a well-known honeycomb structure (see Sect. III.B) and, for each hexagon, we consider the corresponding circle passing through the vertices. As we discuss in the next subsections, such a strategy allows for a convenient triggering and development of the proposed procedure.

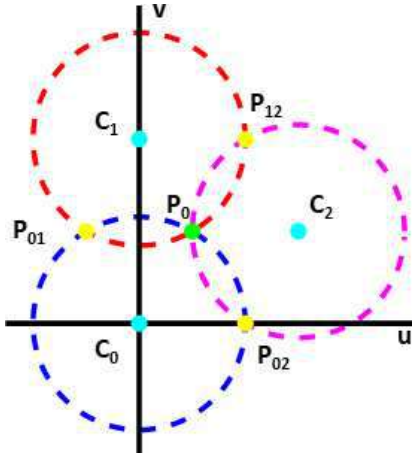

Fig. 1. Pictorial representation of the triggering of the proposed procedure. The signals' value at P_0 (green marker) is used to set a reference phase for the three sets of possible solutions along the circles, while P_{01}, P_{02}, P_{12} (yellow markers) are used as discrimination points, and the signals' values there attained are exploited to discard incongruent solutions. In this configuration, the centers of the three circles are as follows:
$C_1=\sqrt{3k}\left(\cos\frac{\pi}{2},\sin\frac{\pi}{2}\right)$,$C_2=\sqrt{3k}\left(\cos\frac{\pi}{6},\sin\frac{\pi}{6}\right)$, $C_0=(0,0)$.

positioned on (translated from or to) a circle centered in the origin by using suitable linear phases on the source aperture. Therefore, representations given in [2] exactly apply.

III.B. Triggering and development of the PR procedure

By virtue of (1) and (2) as applied to a generic circle of radius $\overline{k}$, one can trigger the overall procedure by considering two or even more very-low-order PR problems. For example, one can consider the three rings of Fig. 1 and ascertain congruence amongst different possible solutions by enforcing (within some tolerance) the following condition:

$$\sum_{\ell=-2H}^{2H} D_\ell(\overline{k}) z^\ell = M^2(\overline{k},\phi) \tag{5}$$

where H is fixed as recalled in Sect. II. As a possible alternative, one can eventually fix it in such a way that H is the minimum number allowing a fitting of the available data.

As it can be seen in Fig. 1, the three rings have a common point, i.e., P_0, which will be used as a reference for phase normalization (e.g., for the choice of the phase reference) as well as three intersection points amongst two of the circles, i.e., P_{01}, P_{02}, P_{12}. These latter will be used for discriminating amongst acceptable or non-acceptable field solutions along the rings[4].

To describe the proposed procedure, let us denote with N_q the number of congruent solutions remaining after that the rings $C_1,C_2,\ldots,C_q$ have been exploited. Moreover, let us denote with $\{S_0^j, S_1^j, \ldots, S_q^j\}_{j=1,\ldots,N_q}$ such a set of solutions, where S_i^j denotes the j-th solution along the i-th ring.

We start the procedure by considering the ring C_0 along which we have N_0 different solutions, say $\{S_0^j\}_{j=1,\ldots,N_0}$. Then, for each of these N_0 solutions, we proceed according to the description in Fig. 2. At the end of this step, we have a number N_1 of admissible couples of solutions, say $\{S_0^i, S_1^i\}_{i=1,\ldots,N_1}$ (see Fig. 2), where $\{S_1^i\}$ refers to the i-th solution along the ring C_1. Note that N_1 may be greater, equal, or (hopefully) smaller than N_0. In fact, when more than one solution on C_1 is compatible with a solution on C_0, the number of possibilities increases, whereas whenever a solution on C_0 has no match with solutions on C_1, it is dropped (thus negatively contributing to the overall number of possible solutions). Once this task has been performed, for each of the admissible couples we enter in the flowchart of Fig. 3 with N=2 [5]. Then, we will have N_2 partial solutions, say $\{S_0^i, S_1^i, S_2^i\}_{i=1,\ldots,N_2}$.

Once again, depending on how many solutions are added (which happens when more solutions on C_2 are compatible with a single couple of solutions along C_0 and C_1) or dropped (which happens when a couple $\{S_0,S_1\}$ has no compatibility with solutions on C_2), N_2 may be larger, equal or (hopefully) smaller than N_1.

[4] Note that, if $H = 1$, one has just four possible field solutions along each ring [2], so that a total of 64 possible configurations have to be checked. Such a number grows to 16^3= 4096 for $H = 2$. However, in most cases one will not really need to explore all of them, as any intersection point provides a pruning of the set of possibilities.

[5] N written without any subscript indicates that the ring C_N is being processed or, which is the same, that the N-th step of the procedure is being performed.

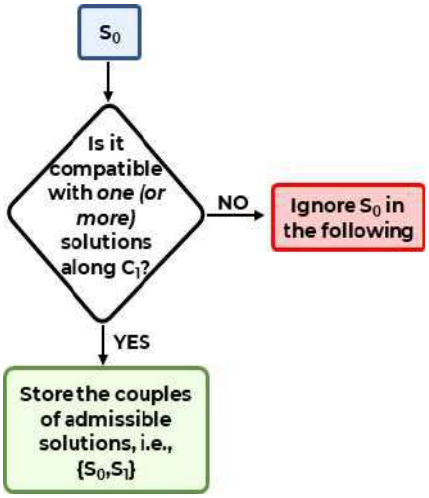

Fig. 2: Triggering procedure: flowchart of the elementary bricks of step 1. The routine must be repeated for each admissible solution S_0 along C_0.

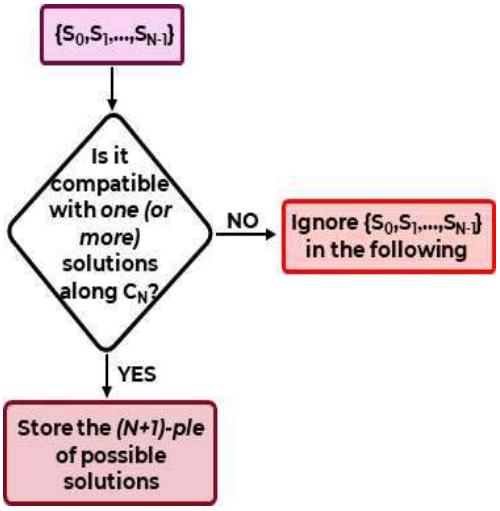

Fig. 3. Flowchart of the *N*-th step of the procedure. The routine must be repeated for each admissible *N*-tuple of solutions along the previously considered rings, i.e., $S_0, S_1, \ldots, S_{N-1}$.

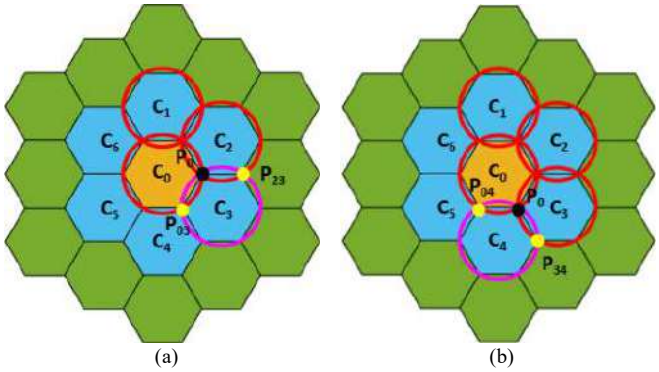

Fig. 4. Pictorial representation of the rationale of the proposed strategy, where subplots (a) and (b) represent two consecutive steps. Along the red lines the complex field has already been retrieved, while in the magenta line it has yet to be recovered. The field value at P_0 (black marker) is used to set a reference phase for all the signals along the circles, while the field values at P_{03}, P_{23} in subplot (a) or P_{04}, P_{34} in subplot (b) (yellow markers) are used as discrimination points to discard incongruent solutions.

The prosecution of the procedure is conceptually simple. In fact, one can consider additional concatenating rings passing through points where the field reconstruction has already been achieved and implementing for each of them the procedure summarized in the flowchart of Fig. 3. For example, by referring to Fig. 4, one can proceed along the blue hexagons, and then progressively consider the hexagons with the next color, and so on. Once the last circle of the 'color group' is included, one may achieve a single couple of complex conjugate solutions along each 1-D cut or, which is usually the case, a number of trial solutions survive. Such a case is not anyway an issue for the overall procedure. In fact, by moving into the next 'color group' it is still possible to prune the tree of possible solutions along the different circles by means of congruence arguments.

As already noted, each level of the tree of all possible partial solutions may have a number of branches higher, equal, or lower than at the previous level. In case of noiseless data, and apart from the case of factorable fields, one will end with a single (complex conjugate) couple of solutions.

Also note that a further hypothesis which is used throughout is that the spectrum is negligible in its invisible part (otherwise an infinite number of circles would be needed).

Finally, once the actual (plus its complex conjugate) solution is available for any circle covering the visible part of the spectrum, and provided the circles are sufficiently dense, interpolation or fitting of the optimal representation for the spectrum (see eq. (22) of [2]) will conclude the procedure[6].

III.C. Implementation details

This subsection discusses three relevant details of the procedure, i.e., the data extraction along the non-concentric rings, the optimal choice of the radius $\overline{k}$, and the management of the discrimination process at the intersecting points.

The first issue arises from the fact that, in order to solve the PR problem along different non-concentric rings, one needs a square-amplitude representation of the data as prescribed by equation (4). This is a necessary condition to apply the SF technique [28] and find the different candidate solutions along each ring. To this end, one can compute the actual square-amplitude samples in $4H+1$ equispaced points along the ring, and then perform a Discrete Fourier Transform (DFT) that will generate the required $D_p(\overline{k})$ values. As far as the computation of the samples is concerned, different methods can be used.

As a first and more obvious choice, if (u_d, v_d) is the point of the spectral plane where the value of M^2 is required, one can rely on the explicit computation of the cardinal series representation. However, if no Fast Fourier Transform (FFT) is used, such a choice can be computationally intensive in case of large sources.

A faster procedure takes advantage from the effectiveness of FFT codes. In fact, starting from the initial samples and using FFT, zero padding, and inverse FFT, one can get an interpolation of the M^2 distribution on a much denser grid. In

[6] While the procedure is running, we only retrieve the solutions on the circles whereas the field inside them actually depends on the remaining (external) samples that have to be recovered. As a result, it is just at the end of the procedure that one ends up with an overall retrieval.

such a way, one is able to make the power pattern available at points as close as desired to the ring at hand. Then, by using the points of the grid closest to the ring (and neglecting the distance from the ring itself), one can proceed to a best fitting procedure amongst representation (4) (with $z = e^{j\phi}$) and the values of M^2 on the closest points. Notably, a sufficiently dense grid (see below) and the relatively low value of H (which allows for filtering high frequency errors) allow to neglect the inherent approximation error.

A third intermediate possibility, starting again from the Nyquist grid samples, amounts in computing the field (spectrum) on a denser grid by using a FFT-based computation. Then, one of the self-truncating sampling series of [32] can be used. For any desired (u_d, v_d) point, the latter will allow getting the required value by using a summation over a limited number of nearby sampling points of the dense grid.

In the numerical analysis which follows, the second strategy is exploited. In particular, in all examples we interpolated the measured power pattern on a Cartesian grid which is 32 times denser (along each coordinate) than the initial one (which is taken at a Nyquist rate for the square-amplitude data). Note that in all three methods the truncation of the measurement domain in the spectral plane (as one just can measure the visible part of the spectrum) can imply an interpolation error, which is anyway negligible under the assumed hypothesis of non-superdirective sources. Such an error is absent in case of uniformly spaced arrays (and hence periodic spectra) provided the spacing is sufficiently large (see [27] for more details). Notably, by virtue of the chosen approach, truncation of the invisible part of the spectrum will also be negligible by using a denser measurement grid (as compared to the Nyquist one) in the visible range plus self-truncating interpolation schemes.

A second general relevant issue concerns the choice of the radius $\overline{k}$. In fact, from one side, a very small radius is suggested in order to deal with a low number of combinations to be checked, but then the fields at the different intersection points might not be independent one from each other, thus reducing the discrimination capabilities. On the other hand, a large radius ensures that fields at the intersection points will be independent, but at the expense of an increase of H and, accordingly, of the computational cost.

As a trade-off, we found it convenient to choose a ring radius equal to half of the Nyquist distance [2] (for the unknown spectrum)[7], which leads to $H = \left\lfloor \frac{\pi}{2a} a \right\rfloor = 2$. Notably, thanks to the hexagonal structure depicted in Fig. 4, such a choice also allows to get the samples at a rate higher than the Nyquist one for the spectrum, so that the final reconstruction can be simply performed by interpolation.

The third relevant point is the management of the discrimination (pruning) process at the intersecting points. By the sake of simplicity, let us refer to the case of a generic circle, i.e., the circle C_4 in Fig. 4(b). As it can be seen, one has three intersections with other circles which have been already considered. Then, the central point (i.e., P_0) is used to fix the constant phase ambiguity and the other two intersections are used for discrimination.

In order to assess which solutions are admissible, we compare the unwrapped phases at the discriminating points (as computed on the already considered circles) and the trial ones. In particular, we keep the trial solutions leading to a misfit lower than a given threshold and discard all the other ones. This threshold is calibrated in an empirical way as follows: during the first steps of the crosswords-like procedure, the algorithm progressively increases the threshold and stops as soon as at least two different solutions survive for all the first seven rings (i.e., the rings C_0–C_6 depicted in Fig. 4). Such a threshold is then used for the next 'color group'.

Since in presence of noisy data one has necessarily a misfit at the discrimination points, the problem also arises on which value one has to attribute to the spectrum in the two discrimination points[8]. In this respect, we use in each discrimination point the average value amongst the unwrapped phase as resulting from previous circles and those resulting from the SF on the circle at hand.

III.D. Limitations

The proposed approach is affected by some limitations.

First, if one has a null at an intersection point, then phase makes no sense and hence one cannot use such a point for discrimination purposes. Anyway, apart from very peculiar cases, the other intersection points will allow for some discrimination. Also, one may consider a different ordering of the rings or even a different $\overline{k}$.

Second, if the fields are factorable, the basic procedure furnishes in principle all the different solutions of the problem at hand, which could be a very large number. In fact, factorable fields represent the (zero-measure) set of 2-D cases that is affected by the same kind of ambiguities (related to zero flipping) occurring in the 1-D case. These ambiguities may come into play, leading to a high-number of complex 2-D fields all matching the measured amplitude data. Unfortunately, there is no remedy to such a problem, which is however unlikely in the general case.

A similar limitation arises in the related case when very many partial trial solutions have to be stored and cross-checked with the exploration of new circles. In fact, these cases have a significant impact both on memory requirements and number of needed operations. On the other side, the examples shown in the next Section prove the capability to deal with sources significantly larger than the ones manageable by our previous approaches [1],[2].

Further possible limitations arise in the presence of noisy data. In fact, in such a case the discrimination process may include solutions which do not correspond to the ground truth, or even loose the actual ground truth. However, one has the same risk even using the more usual least square fitting amongst actual data and the trial solution(s)[9]. In this respect,

[7] In fact, a looser grid would be such that some discrimination information may get lost, while a denser grid would be useless.

[8] Which would be P_{04} and P_{34} in the situation depicted in Fig. 4(b).

[9] Saying it according to the 'inverse problems' terminology, even in such a case the generalized solution can be different (and eventually far) from the 'ground truth'.

let us note that, according to our procedure, the final results are anyway compatible with the measured data. In such a framework, the fact we eventually come out with more solutions (rather than one) can allow a further a-posteriori selection according to some additional data or criteria.

Another issue related to noise is the fact that, by virtue of its nature (resembling at large the inversion of a triangular system of linear equations), the procedure could be affected from propagation of errors. However, we did not experience such an issue in the extensive numerical analysis we performed.

Possible improvements such to counteract the above drawbacks are discussed in Sect. V.

IV. NUMERICAL EXAMPLES

In this Section we present some representative outcomes of an extensive set of numerical experiments which have been performed to assess the proposed approach. In particular, three different kinds of radiated fields have been considered dealing respectively with a focused beam from a reflector, a shaped beam from an array of antennas, and the field from a randomly-excited array. In all cases, the size of the source significantly exceeds the ones we have been able to deal with in [1],[2].

In all test cases, to evaluate the impact of noise on the PR accuracy, each square-amplitude data sample has been corrupted by a Gaussian white noise by considering three different values of the signal-to-noise ratio (SNR), i.e., SNR=30dB, SNR=25dB, SNR=20dB. For each test case, according to the implementation details described in Sect. III.C, a different threshold for the unwrapped phase misfit has been identified and adopted. In all cases, the values of $\overline{k}$ and H have been set according to the contents of Sect. III.C.

By denoting with $F_{nominal}$ and $F_{recovered}$ the reference ('ground truth') and retrieved complex field distributions, the outcomes of each experiment have been quantitatively evaluated by using the normalized square error metric for the radiated field (NSE_{rf}) defined as follows:

$$NSE_{rf} = \frac{\|F_{nominal}(u,v) - F_{recovered}(u,v)\|^2}{\|F_{nominal}(u,v)\|^2} \qquad (6)$$

where $u = k'cos\phi$ and $v = k'sin\phi$ are the usual spectral variables (denoting with k' and ϕ the radial and azimuth coordinates spanning the spectral plane).

All reconstructions have been performed by exploiting a computer having an AMD Ryzen Threadripper PRO 3975WX 32-Cores and a 64 GB RAM.

IV.A. Diagnostics of reflector surface deformations

In order to compare the present approach with the one we previously published in [2], the same kind of scenario is considered herein, i.e., the diagnostics of the surface deformation of a reflector antenna. While dealing with the same kind of deformations as in [2], we considered a reflector having a much larger size. In particular, denoting the wavelength by λ, we increased the aperture diameter from 20λ (which was the largest one we were able to manage with the approach in [2]) to 40λ.

Therefore, the reference scenario is the retrieval of a continuous aperture field, say f, having a circular support of radius $a = 20\lambda$, that reads (see also eq. (26)-(27) in [2]):

$$f(\rho', \phi') = |f| e^{j(\varphi_f + \Delta)} \qquad (7)$$

$$|f| = \frac{4FL}{4FL^2 + \rho'^2} \qquad (8)$$

$$\varphi_f = \beta \left[2FL + \tilde{C} \left(\frac{4FL^2 - \rho'^2}{4FL} \right) \right] \qquad (9)$$

$$\Delta = \frac{8FL^2\beta}{4FL^2 + \rho'^2} \delta \qquad (10)$$

wherein ρ' and ϕ' are the radial and azimuth coordinates spanning the aperture, FL represents the focal length, $\tilde{C}$ is a constant chosen as in [5], δ corresponds to the surface deformation of the reflector, and β denotes the wavenumber. Note that in (7) Δ is a space-dependent phase distortion [5] due to a surface deformation δ that adds to the nominal phase φ_f (whereas the source amplitude $|f|$ keeps unaltered).

Coming to details, we set $FL=12\lambda$, $\tilde{C} = 0.5$, and, as in [5], δ as a matrix whose entries are real numbers randomly selected in the range $\left[-\frac{\lambda}{30}, \frac{\lambda}{30}\right]$. Finally, a Gaussian taper has been superimposed to (8) to get an overall 20 dB ratio between the amplitude of the field attained, respectively, at the origin and at the border of the aperture.

The PR in the spectral domain has been performed by exploiting 6924 concatenating rings having a radius equal to half the Nyquist distance and covering the visible space of spectral plane. As the retrieved samples have been taken with a step below the Nyquist one, it has been possible computing the full field matrix by using a simple Fourier interpolation.

The achieved results are summarized in Tab. I, where the three adopted thresholds, the obtained NSE_{rf} values and the corresponding computational times are reported. Furthermore, the difference between reference and retrieved solutions (both in terms of far-field phase and reflector deformation) is shown in Fig. 5 where, by the sake of brevity, just the most cumbersome case with SNR=20 dB is reported.

As it can be seen in Fig. 5 as well as by analyzing the NSE_{rf} values reported in Tab. I, the proposed method has been able to correctly retrieve not only the far-field phase, but also the term related to the reflector deformation. Therefore, the same accuracy performance as in [2] has been achieved by considering, this time, an antenna covering an area that is four times larger.

	Threshold for phase misfit	NSE_{rf}	*Computational Time*
SNR 30dB	8°	$4.15 \cdot 10^{-4}$	roughly 3 hours
SNR 25dB	10°	$5.56 \cdot 10^{-4}$	roughly 4 hours
SNR 20dB	15°	$7.85 \cdot 10^{-3}$	roughly 6 hours

Tab. I. Diagnostics of a reflector surface deformation: performance parameters for different SNR values.

IV.B. Array excitations retrieval for a shaped beam

In order to test the proposed approach on a 'structured' pattern, we considered a square array composed of 3600 isotropic elements located on a uniformly-spaced 60×60 lattice having a 0.707λ inter-element spacing and radiating a flat-top power pattern with a footprint resembling the land of Italy as shown in Fig. 6. The complex excitations generating this power pattern have been synthesized by using the approach introduced in [33].

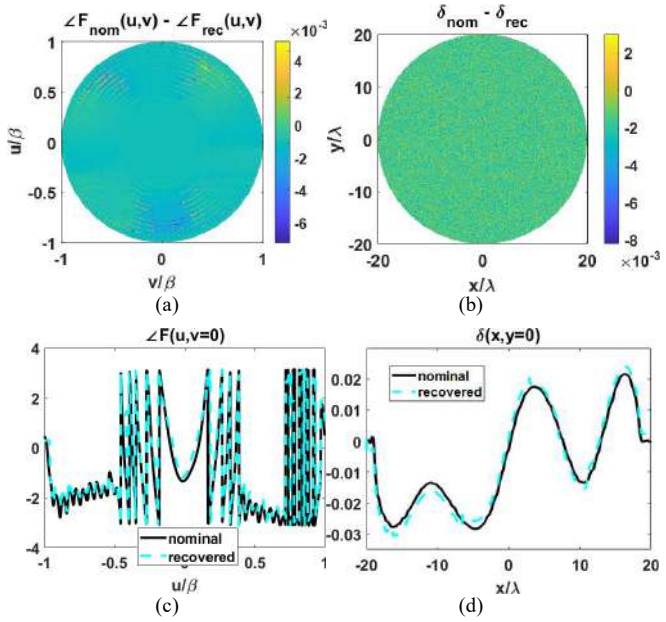

Fig. 5. Diagnostics of a reflector surface deformation leading to a phase distortion on the aperture field in presence of noisy data (SNR=20 dB). Subplot (a): difference between nominal and recovered phases of the far field (radians $\times 10^{-3}$). Subplot (b): difference between nominal and recovered reflector surface deformations (wavelengths $\times 10^{-3}$). Subplot (c): 1-D cut of the nominal (continuous black curve) and recovered (dashed-cyan curve) far-field phases for $v = 0$ (radians). Subplot (d): 1-D cuts of the nominal (continuous black curve) and recovered (dashed-cyan curve) surface deformations along in $y = 0$ (wavelengths).

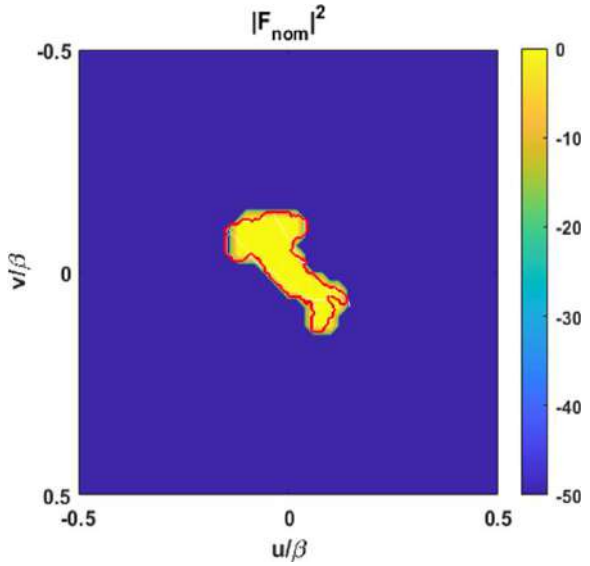

Fig. 6: Italy-like shaped reference power pattern (dB) adopted in subsection IV.B.

To perform the phase retrieval, we considered 7260 concatenating rings of radius still equal to half of the Nyquist distance. The achieved results summarized in Tab. II demonstrate that the procedure again succeeded in finding the actual far-field (and its complex conjugate companion) and the corresponding array excitations. Based on the results in Fig. 7 (where just the most cumbersome case with SNR=20 dB is reported), it can be concluded that the proposed approach is effective even in case of 'structured' electromagnetic fields.

	Threshold for phase misfit	NSE_{rf}	*Computational Time*
SNR 30dB	8°	$5.06 \cdot 10^{-4}$	roughly 4 hours
SNR 25dB	11°	$4.83 \cdot 10^{-4}$	roughly 5 hours
SNR 20dB	14°	$7.41 \cdot 10^{-3}$	roughly 6 hours

Tab. II. Excitations retrieval of a 3600-elements planar array: performance parameters for different SNR values.

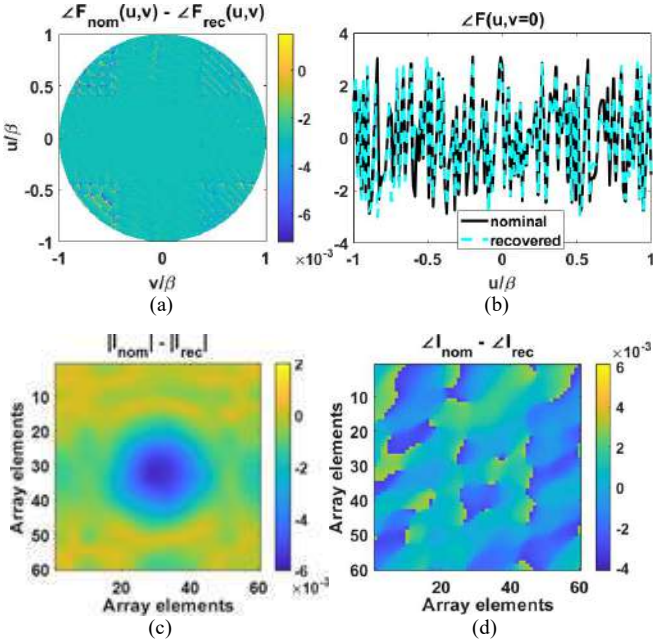

Fig. 7. Retrieval of the complex excitations of the 60×60 planar array generating the power pattern covering the land of Italy as per Fig. 6 (SNR=20 dB). Subplot (a): difference between nominal and recovered phases of the far field (radians $\times 10^{-3}$). Subplot (b): 1-D cut of the nominal (continuous black curve) and recovered (dashed-cyan curve) far-field phases for $v = 0$ (radians). Subplot (c): difference between nominal and recovered excitation amplitudes. Subplot (d): difference between nominal and recovered excitation phases (radians).

IV.C. Excitations retrieval of a large random array

As a final test case, we applied the proposed approach to the same square array[10] described in subsection IV.B wherein, this time, the element excitations have been set as complex numbers whose real and imaginary parts are both randomly selected in the range [-1,1].

The achieved results are summarized in Tab. III. Furthermore, the difference between reference and retrieved

[10] And hence the same number of concatenating rings.

solutions for the most cumbersome case with SNR=20 dB is shown in Fig. 8. As it can be seen, the PR resulted again successful notwithstanding the non-regular behavior of the excitations. This circumstance also proves again the capability of the proposed procedure to deal with a large number of independent unknowns, i.e., with electrically-large radiating systems.

	Threshold for phase misfit	NSE_{rf}	*Computational Time*
SNR 30dB	9°	$3.18 \cdot 10^{-4}$	roughly 4 hours
SNR 25dB	15°	$6.35 \cdot 10^{-4}$	roughly 5 hours
SNR 20dB	15°	$5.12 \cdot 10^{-3}$	roughly 6 hours

Tab. III. Excitations retrieval of a 3600-elements random planar array: performance parameters for different SNR values.

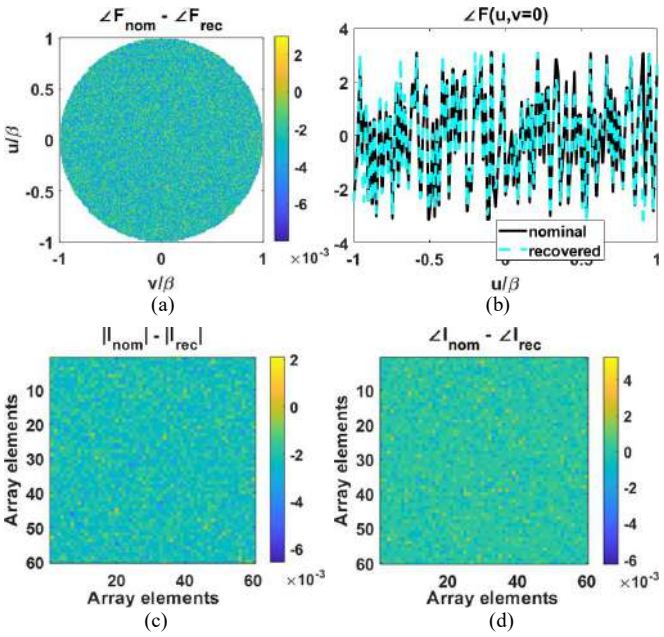

Fig. 8. Retrieval of the complex excitations of the 60×60 planar random array (SNR=20 dB). Subplot (a): difference between nominal and recovered phases of the far field (radians $\times 10^{-3}$). Subplot (b): 1-D cut of the nominal (continuous black curve) and recovered (dashed-cyan curve) far-field phases for $v = 0$ (radians). Subplot (c): difference between nominal and recovered excitation amplitudes. Subplot (d): difference between nominal and recovered excitation phases (radians).

V. Conclusions, and Possible Improvements

An innovative strategy for the effective 2-D phase retrieval of radiated complex fields starting from amplitude-only measurements on a single surface has been presented and assessed.

The proposed procedure takes advantage from the 'crosswords' paradigm proposed and developed in [1],[2],[4] but relies herein on the intersection of curves (i.e., rings) having a much smaller length. Consequently, on these curves one has to deal with fields having a small rate of variability, which correspond to low orders of the associated polynomials and to a small number of possible solutions along each ring. Hence, both each single factorization problem and the pruning of the tree of possible combinations are greatly simplified. In summary, the new choice and the associated procedure allow us to overcome the bottleneck of the related approaches [1],[2],[4].

As suggested by one of the unknown Reviewers, the approach could also be seen as the global optimization/minimization of a cost functional. However, the proposed approach is indeed different from usual global optimization in at least two different characteristics. First, it does not evolve along (and down) the basins of a cost functional, but rather looks 'directly' for the bottom points of the global optima attraction basins. Moreover, while usual global optimization schemes make an extensive use of random search, the proposed approach proceeds in a deterministic fashion, with the inherent advantages.

The overall procedure has been successfully assessed in case of sources different and considerably larger than the ones in [1] and [2], including reflector and array antennas with noisy data. Notably, as opposite to almost all existing methods, it only requires a single measurement set (plus some minimal additional a-priori information able to solve a 1-bit ambiguity [2]) and hence offers definite advantages in terms of measurement time over the more standard 'two-sets-of-data' techniques.

Interestingly, by using the 'reduced radiated field' concept [34], the presented approach can also be used in the case of near-field data. In fact, near fields can also be considered bandlimited provided suitable auxiliary variables (depending on the kind of source and measurement surfaces, as well as on their distance) are introduced.

On the other side, as extensively discussed in subsection III.D, a number of limitations also occur.

As obvious, in case of factorable fields the solution is not unique, so that no algorithm can pretend to recover the ground truth. However, up to a moderate degree of non-uniqueness, the proposed procedure allows in principle to recover the different possible solutions, which is of interest in view of a further potential refinement according to additional data or possible a-priori information.

As far as the difficulties related to the eventual necessity of storing a large set of trial solutions are concerned, a first set of potential improvements arises from possible hybridizations of the present approach with more standard techniques based on the optimization of a cost functional [13],[26]. In fact, the presented approach could give useful starting points for more standard techniques[11], or even useful information to escape from false solutions.

A second set of possibilities arises from the very many degrees of freedom one has at his/her disposal in the way of filling the spectral plane by means of circles, by acting on $\overline{k}$ as well as on the order of filling. Fox example, in order to trigger the procedure, one can choose a triplet of circles other than the one proposed in subsection III.A. Such a degree of freedom suggests that one can consider two or more clusters of rings and solve separately (i.e., in parallel, with definite computational advantages) the problem on the different clusters. In the end, a proper choice of a phase constant

[11] Also note that a post processing based on a cost functional may correct possible propagation of errors.

associated to each cluster will provide the correct concatenation amongst the different parts of the spectrum. Notably, the approach will also be of help in reducing the possible propagation of errors, as well as a better control of the number of trial solutions. Quite interestingly, such a kind of strategy has again another similarity with crosswords puzzles solution schemes.

REFERENCES

[1] G. M. Battaglia, R. Palmeri, A. F. Morabito, P. G. Nicolaci, and T. Isernia, "A non-iteative crosswords-inspired approach to the recovery of 2-D discrete signals from phaseless fourier transform data," *IEEE Open Journal of Antennas and Propagation*, vol. 2, pp. 269-280, 2021.

[2] R. Palmeri, G. M. Battaglia, A. F. Morabito, and T. Isernia, "Reflector antennas characterization and diagnostics using a single set of far-field phaseless data and crosswords-like processing," *IEEE Transactions on Antennas and Propagation*, vol. 70, n. 9, pp. 8424-8439, 2022.

[3] P. J. Napier and R. H. T. Bates, "Inferring phase information from modulus information in two-dimensional aperture synthesis," *Astronomy and Astrophysics Supplement Series*, vol. 15, p. 427, 1974.

[4] H. V. Deighton, M. S. Scivier, and M. A. Fiddy, "Solution of the two-dimensional phase-retrieval problem," *Optics letters*, vol. 10, n. 6, pp. 250-251, 1985.

[5] L. Taylor, "The phase retrieval problem," *IEEE Transactions on Antennas and Propagation*, vol. 29, n. 2, pp. 386–391, 1981.

[6] J. R. Fienup, "Phase retrieval algorithms: a comparison," *Applied optics*, vol. 21, n. 15, pp. 2758-2769, 1982.

[7] D. Morris, "Phase retrieval in the radio holography of reflector antennas and radio telescopes," *IEEE Transactions on Antennas and Propagation*, vol. 33, n. 7, pp. 749-755, 1985.

[8] Y. Rahmat-Samii, "Microwave holography of large reflector antennas-simulation algorithms," *IEEE Transactions on Antennas and Propagation*, vol. AP-33, n. 11, pp. 1194–1203, 1985.

[9] R. P. Millane, "Phase retrieval in crystallography and optics," *Journal of the Optical Society of America A*, vol. 7, n. 3, pp. 394–411, 1990.

[10] R. M. Von Bunau, H. Fukuda, and T. Terasawa, "Phase retrieval from defocused images and its applications in lithography," *Japanese Journal of Applied Physics*, vol. 36, n. 12S, p. 7494, 1997.

[11] G. Leone and R. Pierri, "Reflector antenna diagnosis from phaseless data," *IEEE Transactions on Antennas and Propagation*, vol. 45, n. 8, pp. 1236-1244, 1997.

[12] R. Pierri, G. D'Elia, and F. Soldovieri, "A two probes scanning phaseless near-field far-field transformation technique," *IEEE Transactions on Antennas and Propagation*, vol. 47, n. 5, pp. 792–802, 1999.

[13] T. Isernia, G. Leone, and R. Pierri, "Phase retrieval of radiated fields," *Inverse Problems,* vol. 11, n. 1, pp. 183-203, 1999.

[14] S. Costanzo, G. Di Massa, and M. D. Migliore, "A novel hybrid approach for far-field characterization from near-field amplitude-only measurements on arbitrary scanning surfaces," *IEEE Transactions on Antennas and Propagation*, vol. 53, n. 6, pp. 1866-1874, 2005.

[15] S. Marchesini, "A unified evaluation of iterative projection algorithms for phase retrieval," *Review of scientific instruments*, vol. 78, n. 1, 2007.

[16] A. Capozzoli, C. Curcio, G. D'Elia, and A. Liseno, "Phaseless antenna characterization by effective aperture field and data representations," *IEEE Transactions on Antennas and Propagation*, vol. 57, n. 1, pp. 215-230, 2009.

[17] R. K. Amineh, J. McCombe, and N. K. Nikolova, "Microwave holographic imaging using the antenna phaseless radiation pattern," *IEEE Antennas and Wireless Propagation Letters*, vol. 11, n. 1, pp. 529-1532, 2012.

[18] G. Junkin, "Planar near-field phase retrieval using GPUs for accurate THz far-field prediction," *IEEE Transactions on Antennas and Propagation*, vol. 61, n. 4, pp. 1763-1776, 2013.

[19] B. Fuchs and L. Le Coq, "Excitations retrieval of microwave linear arrays from phaseless far field data", *IEEE Transactions on Antennas and Propagation*, vol. 63, n. 2, pp. 748-752, 2015.

[20] Y. Xu, Q. Ye, and G. Meng, "Optimisation of phase factor in phase retrieval for reflector antennas with active surface," *IET Microwaves, Antennas and Propagation*, vol. 12, n. 15, pp. 2285-2291, 2018.

[21] H. Jin, J. Huang, Q. Ye, G. Meng, B. Xiang, and N. Wang, "Surface shape detection with a single far-field intensity by combined amplitude and phase retrieval," *International Journal of Antennas and Propagation*, vol. 2019, 2019.

[22] R. Moretta and R. Pierri, "Performance of Phase Retrieval via Phaselift and quadratic inversion in circular scanning case," *IEEE Transactions on Antennas and Propagation*, vol. 67, n. 12, pp. 7528-7537, 2019.

[23] J. Knapp, A. Paulus, and T. F. Eibert, "Reconstruction of squared field magnitudes and relative phases from magnitude-only nearfield measurements," *IEEE Transactions on Antennas and Propagation*, vol. 67, n. 5, pp. 3397–3409, 2019.

[24] R. Palmeri, T. Isernia, and A. F. Morabito, "Diagnosis of planar arrays through phaseless measurements and sparsity promotion," *IEEE Antennas and Wireless Propagation Letters*, vol. 18, n. 6, pp. 1273–1277, 2019.

[25] O. M. Bucci, C. Gennarelli, and C. Savarese, "Representation of electromagnetic fields over arbitrary surfaces by a finite and nonredundant number of samples," *IEEE Transaction on Antennas and Propagation*, vol. 46, n. 3, pp. 351-359, 1998.

[26] T. Isernia, F. Soldovieri, G. Leone, and R. Pierri, "On the local minima in phase reconstruction algorithms," *Radio Science*, vol. 31, n. 6, pp. 1887-1899, 1996.

[27] A. F. Morabito, R. Palmeri, V. A. Morabito, A. R. Laganà, and T. Isernia, "Single-surface phaseless characterization of antennas via hierarchically ordered optimizations," *IEEE Transactions on Antennas and Propagation*, vol. 67, n. 1, pp. 461-474, 2019.

[28] T. Isernia, O. M. Bucci, and N. Fiorentino, "Shaped beam antenna synthesis problems: feasibility criteria and new strategies," *Journal of Electromagnetic Waves and Applications*, vol. 12, n. 1, pp. 103-138, 1998.

[29] A. F. Morabito, L. Di Donato, and T. Isernia, "Orbital angular momentum antennas: understanding actual possibilities through the aperture antennas theory," *IEEE Antennas and Propagation Magazine*, vol. 60, n. 2, pp.59-67, 2018.

[30] O. M. Bucci, L. Crocco, and T. Isernia, "Improving the reconstruction capabilities in inverse scattering problems by exploitation of close-proximity setups," *Journal of the Optical Society of America A*, vol. 16, n. 7, pp. 1788-1798, 1999.

[31] K. Knopp, "Weierstrass's factor-theorem," *Theory of Function*s: Part II, Dover, pp. 1–7, 1996.

[32] O. M. Bucci and G. Di Massa, "The truncation error in the application of sampling series to electromagnetic problems," *IEEE Transactions on Antennas and Propagation*, vol. 36, n. 7, pp. 941-949, 1988.

[33] G. M. Battaglia, A. F. Morabito, G. Sorbello, and T. Isernia, "Mask-Constrained Power Synthesis of Large and Arbitrary Arrays as a Few-Samples Global Optimization," *Progress In Electromagnetics Research C*, vol. 98, pp. 69-81, 2020.

[34] O. M. Bucci and M. D'Urso, "Power pattern synthesis of given sources exploiting array methods," *Proceedings of the Second European Conference on Antennas and Propagation,* pp. 11-16, 2007.